Electronic Supplementary Material (ESI) for Materials Horizons.

Bio-inspired Reliable Manipulation of Gas Bubbles on Interfaces by Regulating Their Microstructures and Chemical Components

Peipei Zhang,[a] Jingjing Zhang,[a] Zhongxin Xue,[b] Jingming Wang*[a] and Lei Jiang[ac]

a. Key Laboratory of Bio-Inspired Smart Interfacial Science and Technology of Ministry of Education, School of Chemistry and Environment, Beihang University, Beijing, 100191, P.R. China.
b. School of Chemistry and Materials Science, Ludong University, Yantai, 264025, P.R. China.
c. Laboratory of Bio-inspired Smart Interface Science, Technical Institute of Physics and Chemistry, Chinese Academy of Science, Beijing, 100190, P.R. China.

Supporting Information 1: The design of the interfaces with different gas bubble behaviors (gas superwettability) for various applications

Table S1 Applications of the interfaces with different gas bubble behaviors (gas superwettability)

Superwettability of gas bubbles	**Application**	**Characters of functional interfaces**	***References***
Superaerophobicity (Bubble repellence) Interfaces with tiny gas bubble release diameter and ultra-weak gas bubble adhesion force	Hydrogen Evolution Reaction (HER)	Pine-shaped Pt nanoarray	*Adv. Funct. Mater.* **2015**, *25*, 1737–1744
		Vertically aligned MoS_2 nanoplates (200 nm in size and less than 5 nm in thickness)	*Adv. Mater.* **2014**, *26*, 2683–2687
		Ultrathin Ni nanosheet arrays (2.2 nm)	*Angew. Chem. Int. Ed.* **2016**, *55*, 693 –697
		Amorphous MoS_2 porous thin film constructed by nanosheets with the size of several micrometers	*Chem. Commun.,* **2013**, *49*, 7516--7518
		Cu_3P microsheets (lateral size: 6 μm, thickness: 510 nm)	*Adv. Mater. Interfaces* **2016***, 3,* 1600236
		NiMo alloy (isolated hemispherical structure with abundant protrusions)	*Small* **2016**, *12,* 2492–2498
	Hydrazine Oxidation Reaction (HzOR)	Vertically aligned Cu nanoplate array (average size: 500 nm, thickness: 50 nm)	*Adv. Mater.* **2015**, *27*, 2361–2366
		Ni nanoflower electrodes	*Nano Res.* **2015**, *8*, 3365–3371.
		Ultrathin Ni nanosheet arrays (thickness: 2.2 nm)	*Angew. Chem. Int. Ed.* **2016**, *55*, 693 –697
		3D porous Ni–Cu alloy film (400 nm flower-like nanostructure)	*Nanoscale* **2016**, **8**, 1479–1484

	Chlorine Evolution Reaction (ClER)	RuO_2@TiO_2 nanosheet array (Irregular sheet-like units with lateral size of 200 nm and thickness of 20 nm)	*Small* **2017**, *13*, 1602240
	Oxygen Evolution Reaction (OER)	$ZnxCo_{3-x}O_4$ nanostructures constructed with secondary nanoneedles grown on primary rhombusshaped pillar arrays (pillar length: 15μm)	*Chem. Mater.* **2014**, *26*, 1889−1895
		Cu_3P microsheets (lateral size 6 μm, thickness is 510 nm)	*Adv. Mater. Interfaces* **2016**, *3*, 1600236
		NiFe-LDH nanoplates (500 nm) vertically grown on Ni foam	*Small* **2016**, *12*, 2492–2498
Hydrophilic/aerophobic	Bubble-assisted (H_2 or O_2) electrodeposition processes	Nanotube-decorated polymer surfaces (without the aid of surfactants)	*J. Mater. Chem. A* **2016**, *4*, 17308–17323
Superaerophilic Interfaces with trapped gas layer and ultra-high gas bubble adhesion force	Oxygen Reduction Reaction (OER)	Porous cobalt-incorporated nitrogen-doped carbon nanotube (CoNCNT) arrays on carbon-fiber paper (CFP)	*Adv. Mater.* **2016**, *28*, 7155-7161
	Enzyme Biosensor	Pt particles (50 to 300 nm) on carbon fiber substrate (diameter: 10 μm)	*Adv. Mater.* **2016**, *28*, 1477–1481
Janus membrane with asymmetric gas wettability	Fine Bubble Aeration	Polypropylene membrane: one side: PDA/PEI-modified, superaerophobic the other side: unmodified surface, aerophilic	*Adv. Mater. Interfaces* **2016**, 1500774

Supporting Information 2: SEM side view images of the silicon surfaces with different microstructures (MSis, NSis and MNSis).

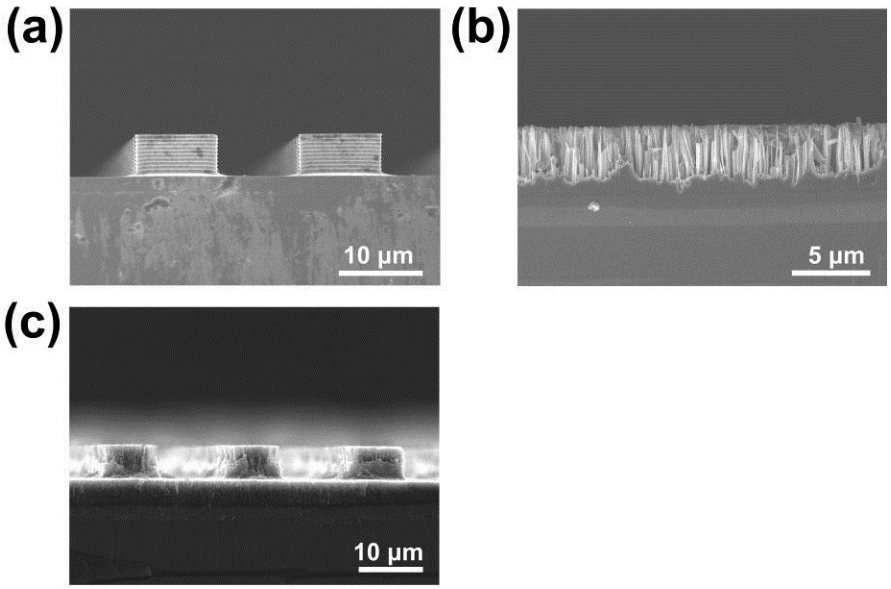

Fig. S1 SEM side view images of the silicon surfaces with different microstructures (a) MSis (W/H/D = 10/5/10 μm); (b) NSis; and (c) MNSis (W/H/D = 10/5/10 μm).

Supporting Information 3: Water CAs of the hydrophobic silicon surfaces with different microstructure.

Fig. S2 Water CAs of hydrophobic surfaces with different micro-structures (a) MSis (W/H/D = 10/5/10 μm); (c) NSis; and (d) MNSis (W/H/D = 10/5/10 μm).

Supporting Information 4: **Video 1** Gas bubble behavior on the SSis interface

Supporting Information 5: **Video 2** Gas bubble behavior on the FAS-SSis interface

Supporting Information 6: **Video 3** Gas bubble behavior on the MSis interface

Supporting Information 7: **Video 4** Gas bubble behavior on the FAS-MSis interface

Supporting Information 8: **Video 5** Gas bubble behavior on the NSis interface

Supporting Information 9: **Video 6** Gas bubble behavior on the FAS-NSis interface

Supporting Information 10: **Video 7** Gas bubble behavior on the MNSis interface

Supporting Information 11: **Video 8** Gas bubble behavior on the FAS-MNSis interface

Supporting Information 12: Series of video snapshots of representative gas bubble behavior from generation to departure on the hydrophobic MSis, NSis and MNSis interfaces.

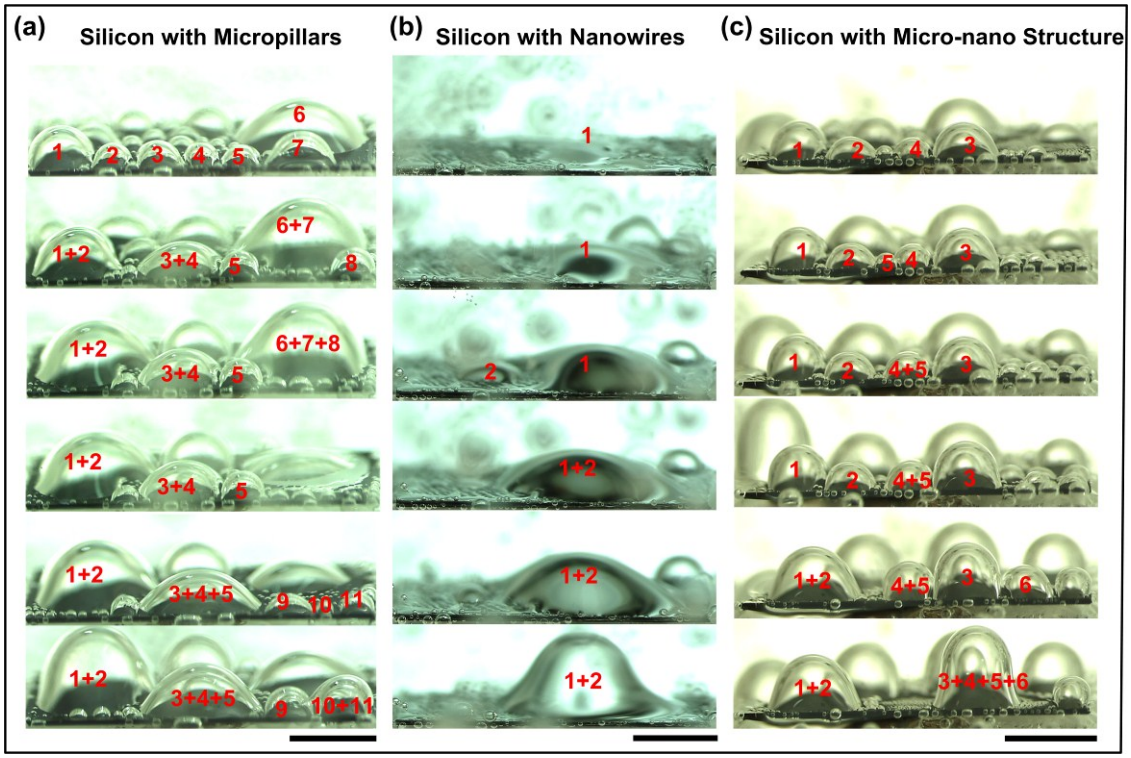

Fig. S3 CO_2 bubble growth processes on the hydrophobic interfaces with different microstructures (a) MSis (W/H/D = 10/5/10 μm); (b) NSis; and (c) MNSis (W/H/D = 10/5/10 μm). The scale bars are 5 mm.

Supporting Information 13: Departure diameters of CO_2 bubbles on the hydrophobic interfaces with different microstructures (MSis10, NSis and MNSis10)

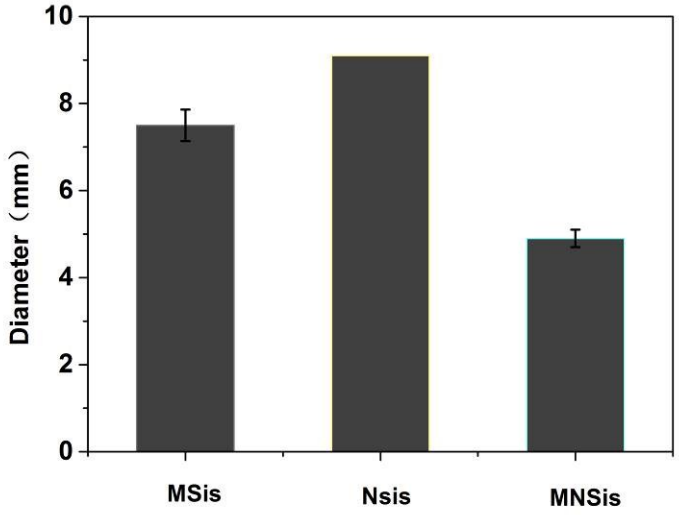

Fig. S4 The departure diameters of CO_2 bubbles on the hydrophobic interfaces with different microstructures (MSis10, NSis and MNSis10).

Supporting Information 14: The adhesion forces between the CO_2 bubbles and the hydrophilic interfaces before FAS-modification.

Fig. S5 illustrates the adhesion force between CO_2 bubbles and the hydrophilic interfaces with different microstructures. The adhesion forces on the SSis and MSis interfaces are close to 0, while the adhesion force on the Nsis and MNSis are a bit larger than 0. During the process of adhesion force measurement, the CO_2 bubbles were fixed on a superhydrophobic copper cap. The distance that the copper cap moved down is 2 mm. It is a bit larger than the diameter of CO_2 bubbles. The bubble volume suspended on the copper cap is 10 μL. Bubble diameter is 2.68 mm. Thus, as the hydrophilic interfaces approach the CO_2 bubble, the CO_2 bubble will be squeezed, and part of the bubble permeated into the nanowire structures. When the bubbles left the surface, the adhesion force increased due to the capillary force.

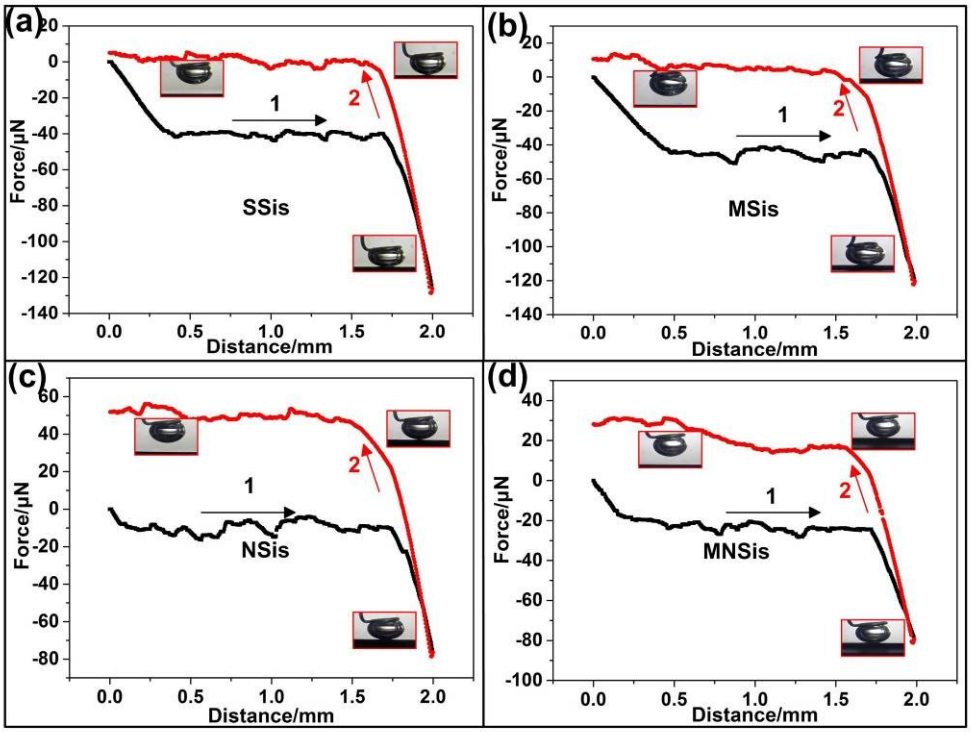

Fig. S5. The adhesion forces between CO_2 bubbles and hydrophilic interfaces with different structures before FAS-modification. (a) SSis; (b) MSis (W/H/D = 10/5/10 μm); (c) NSis; and (d) MNSis (W/H/D = 10/5/10 μm). The inset shows the photographs of the shapes of the CO_2 bubbles taken at the corresponding stages during the measurement process. Process 1: the hydrophilic interfaces approach the CO_2 bubble; Process 2: the hydrophilic interfaces leave the CO_2 bubble.

Supporting Information 15: The adhesion forces between the CO_2 bubbles and the hydrophobic interfaces after FAS-modification.

Fig. S6 shows the record force–distance curves between CO_2 bubbles and the hydrophobic interfaces with different microstructures. The maximum adhesion forces of the hydrophobic interfaces are larger than 200 μN.

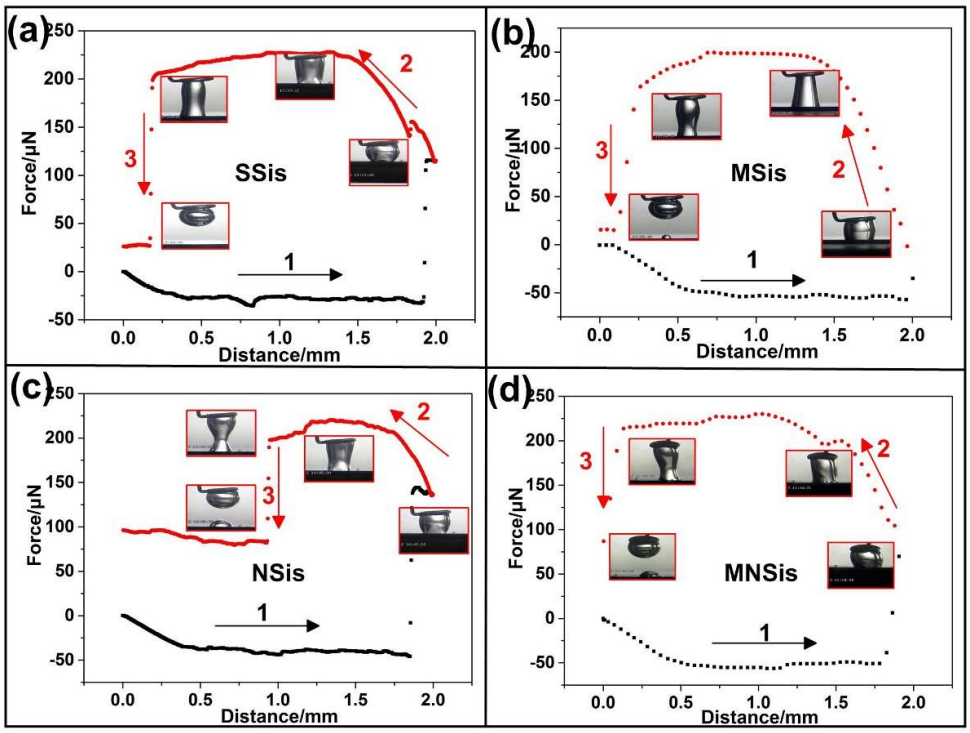

Fig. S6 The adhesion forces between CO_2 bubbles and the hydrophobic interfaces with different microstructures after FAS-modification. (a) FAS-SSis; (b) FAS-MSis (W/H/D = 10/5/10 μm); (c) FAS-NSis; and (d) FAS-MNSis (W/H/D = 10/5/10 μm). The inset shows the photographs of the CO_2 bubble shapes taken at the corresponding stages during the measurement process. Process 1: the hydrophobic interfaces approach the CO_2 bubble; Process 2: the hydrophobic interfaces leave the CO_2 bubble; and Process 3: the hydrophobic interfaces surface break away from the CO_2 bubble.

Supporting Information 16: The adhesion forces between the CO_2 bubbles and the superhydrophobic interfaces after FAS-modification.

Fig. S7 shows the record force-distance curves during the measuring process between CO_2 bubbles and the superhydrophobic interfaces with different microstructures. The maximum forces were larger than 600 μN. The adhesion force on MNSis interface was closed to 1000 μN. From the inset photographs of the CO_2 bubble shapes taken at the corresponding stages, we can see that the bubbles left the superhydrophobic surfaces with parts of bubbles pinned to the surface. The force is the bubble breaking force. The adhesion forces on the superhydrophobic interfaces are larger than the test results.

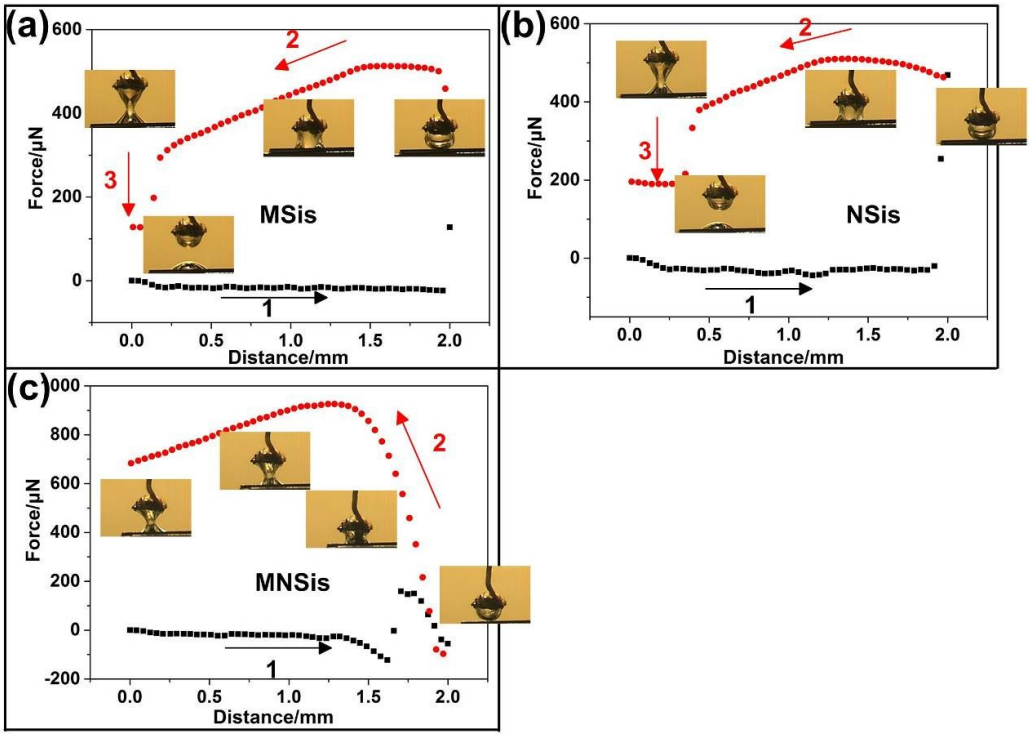

Fig. S7 The adhesion forces between CO_2 bubbles and the superhydrophobic interfaces with different microstructures after FAS-modification. (a) FAS-MSis (W/H/D = 10/5/10 μm); (b) FAS-NSis; and (c) FAS-MNSis (W/H/D = 10/5/10 μm). The inset shows photographs of the CO_2 bubble shapes taken at the corresponding stages during the measurement process. Process 1: the superhydrophobic interfaces approach the CO_2 bubble; Process 2: the superhydrophobic interfaces leave the CO_2 bubble; Process 3: the superhydrophobic interfaces surface break away from the CO_2 bubble.

Supporting Information 17: SEM images of the substrate with different width of micropillars

In order to confirm the influence of the micropattern size on the CO_2 bubble behaviors, we selected another two kinds of micropillars with different width. They are MSis5 (W/H/D = **5**/5/10 μm), MNSis5 (W/H/D=**5**/5/10 μm), MSis15 (W/H/D=**15**/5/10 μm) and MNSis15 (W/H/D=**15**/5/10 μm). Their SEM top and side view images are shown in Fig. S8 and S9.

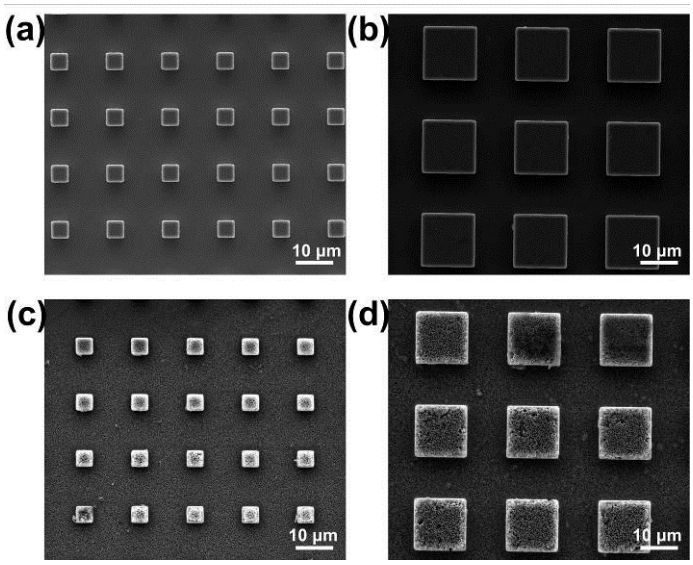

Fig. S8 SEM top view images of the substrate with different width of micropillars (a) Msis5 (W/H/D = 5/5/10 μm) (b) Msis15 (W/H/D = 15/5/10 μm); (c) MNSis5 (W/H/D = 5/5/10 μm); and (d) MNSis15 (W/H/D = 15/5/10 μm).

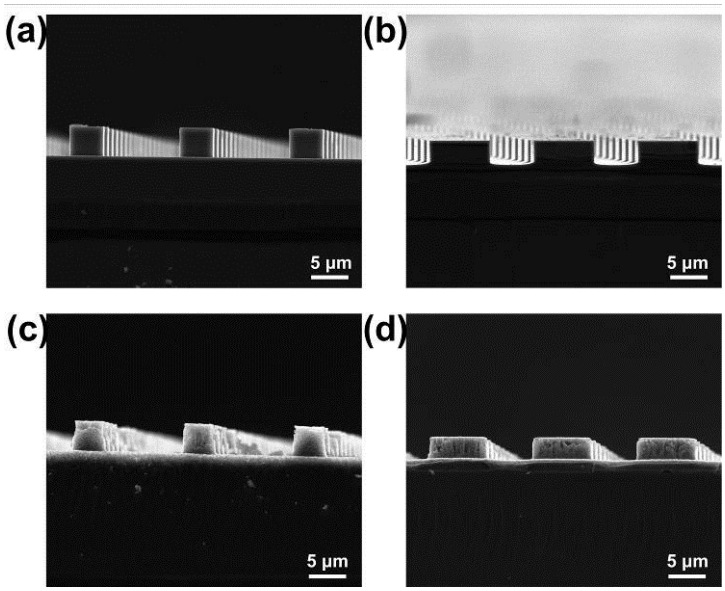

Fig. S9 SEM side view images of the substrate with different width of micropillars (a) Msis5 (W/H/D = 5/5/10 μm) (b) Msis15 (W/H/D = 15/5/10 μm); (c) MNSis5 (W/H/D = 5/5/10 μm); and (d) MNSis15 (W/H/D = 15/5/10 μm).

Supporting Information 18 The CO_2 bubble behaviors on the hydrophohilic, hydrophobic and superhyrophobic interfaces

The in situ CO_2 bubble behaviors on the hydrophohilic (Fig. S10, Fig. S11 and Fig. S12), hydrophobic (Fig. S13, Fig. S14 and Fig. S15) and superhyrophobic (Fig. S16, Fig. S17 and

Fig. S18) interfaces with different width of micropillars, including MSis5, MSis10, MSis15, MNSis5, MNSis10 and MNSis15, were investigated.

On the hydrophilic interfaces, many tiny CO_2 bubbles were generated and grew separately. The grown CO_2 bubbles then escaped from the hydrophilic interfaces with small diameters (Fig. S10). **The diameters of the released CO_2 bubbles on the interfaces with large width of micropillars are larger than that on the interfaces with small width of micropillars.** For example, the diameters of the released CO_2 bubbles on the MSis5, MSis10, MSis15 interfaces were 0.81, 1.20 and 1.24 mm, respectively. After constructing nanostructure on MSis, the diameters of released CO_2 bubbles diseased greatly. The diameters of the released CO_2 bubbles on MNSis5, MNSis10, MNSis15 interfaces dropped to 0.73, 0.77 and 0.84 mm, respectively (Fig. S11). However, the effect of the micropilliar width on the adhesion force between CO_2 bubbles and the hydrophilic interfaces was little (Fig. S12). The adhesion forces on the MNSis interfaces are a bit bigger than those on the MSis interfaces.

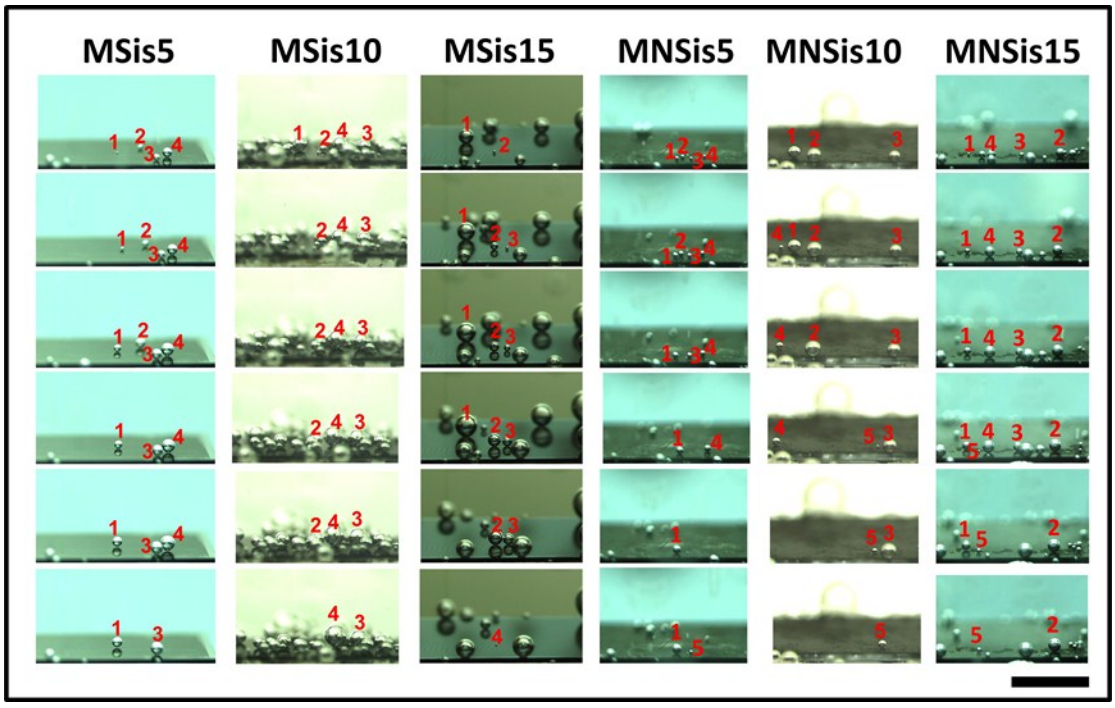

Fig. S10 Series of video snapshots for representative CO_2 bubble growth processes on the hydrophilic interfaces with different width of micropillars, including MSis5 (W/H/D = **5**/5/10 μm), MSis10 (W/H/D=**10**/5/10 μm), MSis15 (W/H/D=**15**/5/10 μm), MNSis5 (W/H/D=**5**/5/10 μm), MNSis10 (W/H/D=**10**/5/10 μm) and MNSis15 (W/H/D=**15**/5/10 μm). The scale bars are 5 mm.

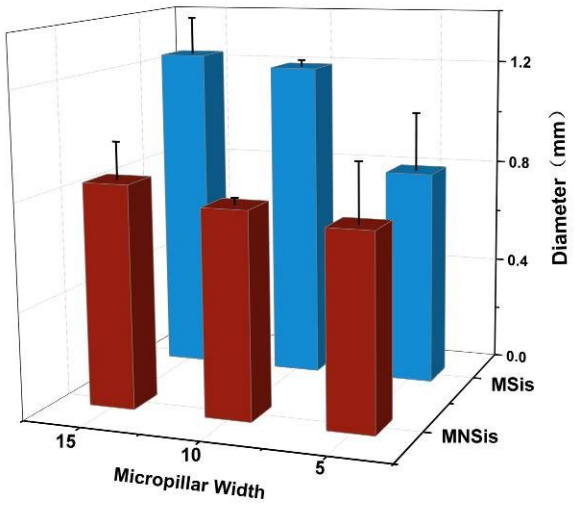

Fig. S11 The departure diameters of CO_2 bubbles on the hydrophilic interfaces with different width of micropillars, including MSis5 (W/H/D = **5**/5/10 μm), MSis10 (W/H/D=**10**/5/10 μm), MSis15 (W/H/D=**15**/5/10 μm), MNSis5 (W/H/D=**5**/5/10 μm), MNSis10 (W/H/D=**10**/5/10 μm) and MNSis15 (W/H/D=**15**/5/10 μm).

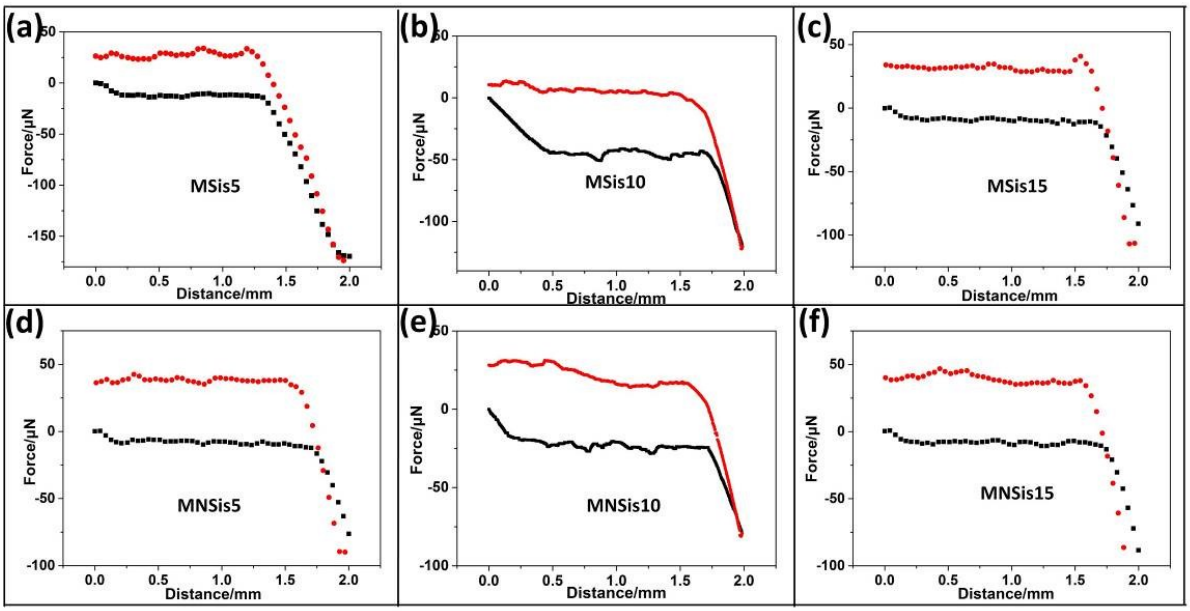

Fig. S12 The adhesion forces between CO_2 bubbles and the hydrophilic interfaces with different width of micropillars, including MSis5 (W/H/D = **5**/5/10 μm), MSis10 (W/H/D=**10**/5/10 μm), MSis15 (W/H/D=**15**/5/10 μm), MNSis5 (W/H/D=**5**/5/10 μm), MNSis10 (W/H/D=**10**/5/10 μm) and MNSis15 (W/H/D=**15**/5/10 μm).

On the hydrophobic interfaces, many CO_2 bubbles with spherical crown shapes are generated. The coalescence could be observed during the bubbles growth process. After the CO_2 bubbles were large enough to overcome the adhesion of the hydrophobic interfaces, they released with spherical crown shapes (Fig. S13). The diameters of the released CO_2 bubbles on the hydrophobic MSis5, MSis10, MSis15 interfaces with different width of micropillars were 3.92, 7.5 and 4.85 mm, respectively. When the nanowire arrays were fabricated on the micropillar interfaces, the diameters of the released CO_2 bubbles on the hydrophobic MNSis5, MNSis10, MNSis15 were 10.16, 4.9 and 10.8 mm (Fig. S14). The adhesion forces on the MSis5, MNSis5 and MNSis15 interfaces were closed to 400 μN, while the adhesion forces on the MSis10, MSis15 and MNSis10 interfaces were only 200 μN, as shown in Fig. S15. We believed that the irregular results of the CO_2 bubble departure diameter and the adhesion forces on hydrophobic interfaces may be cause by our FAS modification method. We adopted the chemical vapor deposition (CVD) to fabricated FAS modified silicon. The difference of

hydrophobicity was achieved by controlling deposition time. The deposition time was 2 h. Due to deposition time is limited, FAS molecules may not been uniformly grafted on the micro and nanostructures of MNSis. Thus, some areas are hydrophobic while some ones are hydrophilic.

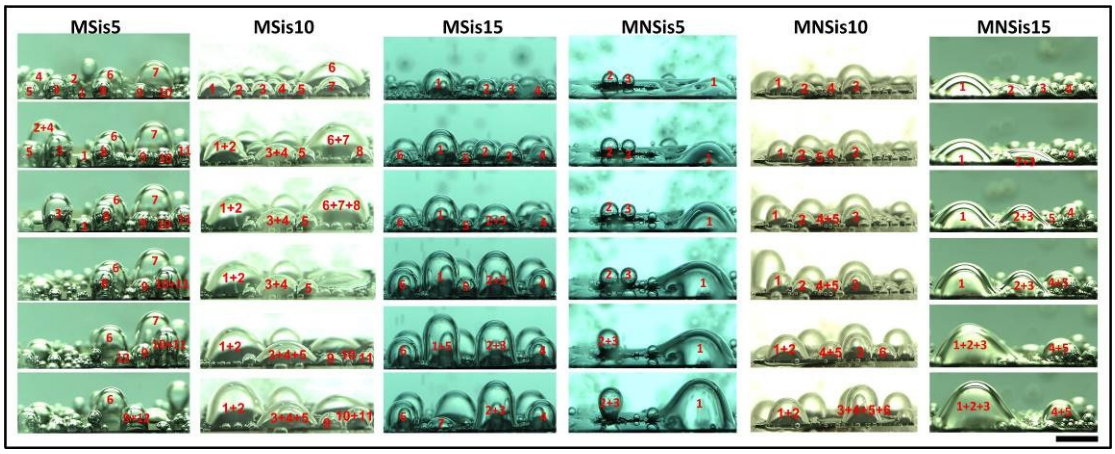

Fig. S13 Series of video snapshots for representative CO_2 bubble growth processes on the hydrophobic interfaces with different width of micropillars, including MSis5 (W/H/D = **5**/5/10 μm), MSis10 (W/H/D=**10**/5/10 μm), MSis15 (W/H/D=**15**/5/10 μm), MNSis5 (W/H/D=**5**/5/10 μm), MNSis10 (W/H/D=**10**/5/10 μm) and MNSis15 (W/H/D=**15**/5/10 μm). The scale bars are 5 mm.

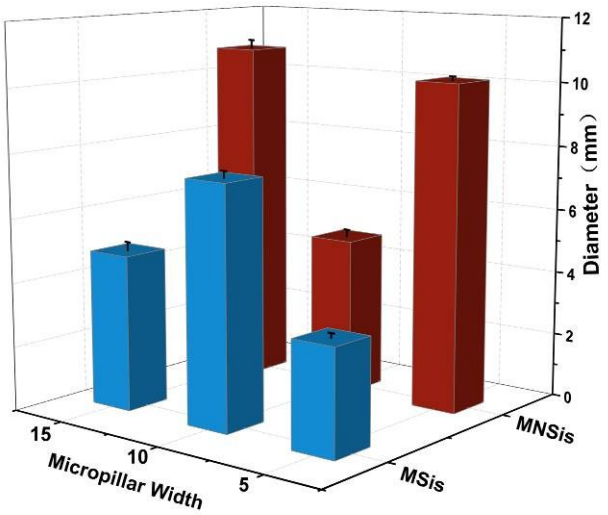

Fig. S14 The departure diameters of CO_2 bubbles on the hydrophobic interfaces with different width of micropillars, including MSis5 (W/H/D = **5**/5/10 μm), MSis10 (W/H/D=**10**/5/10 μm), MSis15 (W/H/D=**15**/5/10 μm), MNSis5 (W/H/D=**5**/5/10 μm), MNSis10 (W/H/D=**10**/5/10 μm) and MNSis15 (W/H/D=**15**/5/10 μm).

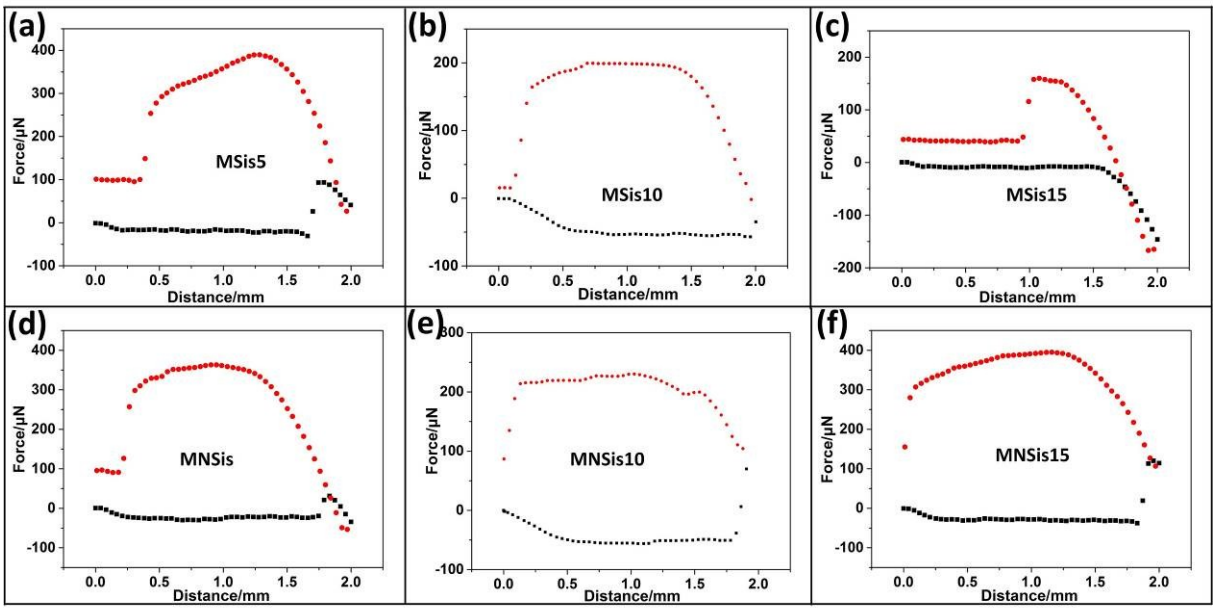

Fig. S15 The adhesion forces between CO_2 bubbles and the hydrophobic interfaces with different width of micropillars, including MSis5 (W/H/D = **5**/5/10 μm), MSis10 (W/H/D=**10**/5/10 μm), MSis15 (W/H/D=**15**/5/10 μm), MNSis5 (W/H/D=**5**/5/10 μm), MNSis10 (W/H/D=**10**/5/10 μm) and MNSis15 (W/H/D=**15**/5/10 μm).

On the superhydrophobic interfaces, a shining CO_2 gas film covered on them. The shining CO_2 gas film slowly bulged out over the interfaces. The bulge then grew higher and higher, and the three-phase contact line (TPCL) shrank. Therefore, the departure diameters of CO_2 bubbles on the superhydrophobic interfaces increased significantly (Fig. S16). On the superhydrophobic MSis interfaces, the diameters of the released CO_2 bubbles increased slightly if the micropillar width increased. When the nanowire arrays were fabricated on the MSis interfaces, the departure diameters of the CO_2 bubbles increase from 8.0, 9.2, and 10.7 mm on the MSis5, MSis10 and MSis15 interfaces to 16.1, 13.8, and 14.7 mm on the MNSis5, MNSis10 and MNSis15 interfaces, respectively (Fig. S17). The adhesion force between CO_2 bubbles and the superhydrophobic interfaces was quite high. The effect of the micropilliar size on the adhesion force was little. The adhesion forces on the MNSis interfaces are much lager than those on the MSis interfaces (Fig. S18).

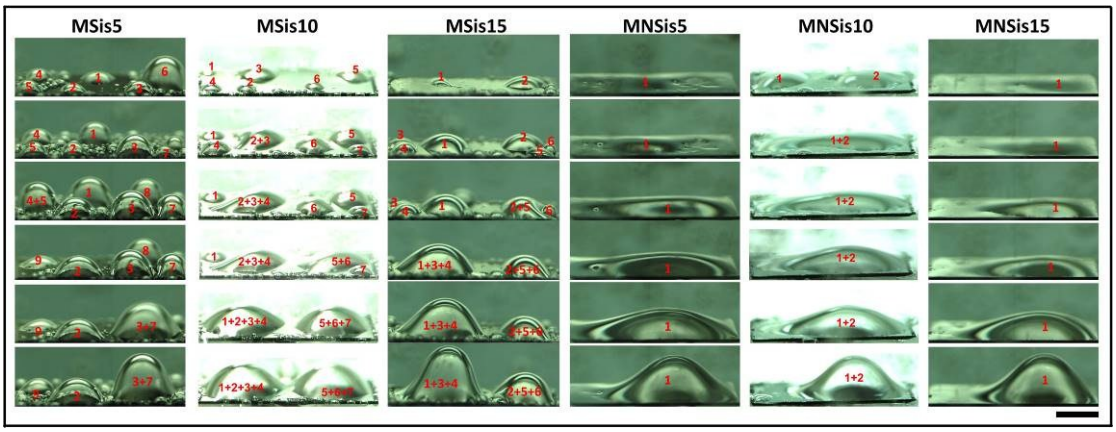

Fig. S16 Series of video snapshots for representative CO_2 bubble growth processes on the superhydrophobic interfaces with different with different width of micropillars, including MSis5 (W/H/D = **5**/5/10 μm), MSis10 (W/H/D=**10**/5/10 μm), MSis15 (W/H/D=**15**/5/10 μm), MNSis5 (W/H/D=**5**/5/10 μm), MNSis10 (W/H/D=**10**/5/10 μm) and MNSis15 (W/H/D=**15**/5/10 μm). The scale bars are 5 mm.

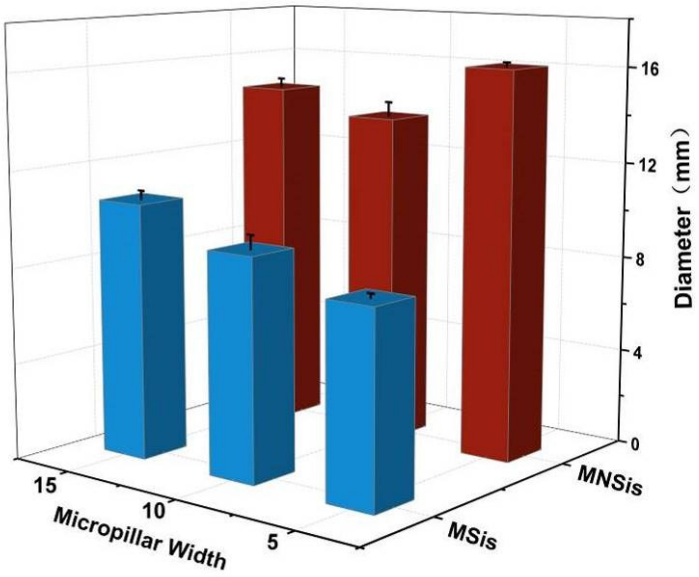

Fig. S17 The departure diameters of CO_2 bubbles on the superhydrophobic interfaces with different width of micropillars, including MSis5 (W/H/D = **5**/5/10 μm), MSis10 (W/H/D=**10**/5/10 μm), MSis15 (W/H/D=**15**/5/10 μm), MNSis5 (W/H/D=**5**/5/10 μm), MNSis10 (W/H/D=**10**/5/10 μm) and MNSis15 (W/H/D=**15**/5/10 μm).

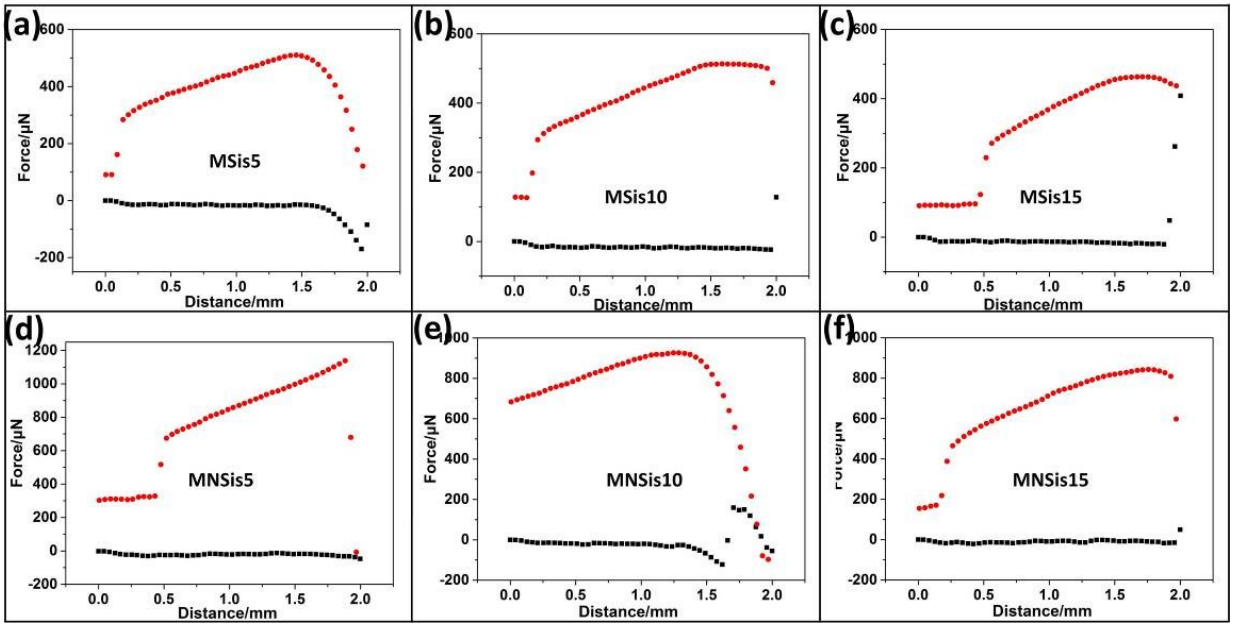

Fig. S18 The adhesion forces between CO_2 bubbles and the superhydrophobic interfaces with different width of micropillars, including MSis5 (W/H/D = **5**/5/10 μm), MSis10 (W/H/D=**10**/5/10 μm), MSis15 (W/H/D=**15**/5/10 μm), MNSis5 (W/H/D=**5**/5/10 μm), MNSis10 (W/H/D=**10**/5/10 μm) and MNSis15 (W/H/D=**15**/5/10 μm).

Therefore, the size of the micropattern (including width, distance and height of the micropillars) could affect the CO_2 bubble behaviors. However, compared with the scale of the rough structures (i.e., microscale and nanoscale), the effect of the micropattern size is not significant. That is to say, the difference of the CO_2 bubble behaviors between the interfaces with different scale of the structures is more significant than that between interface the sizes of microstructures under the same scale.

Supporting Information 19: In the supersaturated solution, CO_2 molecules transfer from the bulk of a supersaturated liquid to a bubble surface. The bubble growth rate k can be calculated as follows:

$$k = \frac{dR}{dt} \approx 0.63 \frac{k_B \mathrm{T}}{P_0} D^{2/3} \left(\frac{2\alpha\rho g}{9\eta}\right)^{1/3} \Delta c \qquad \text{(S1)}$$

Here R is bubble radius, k_B is Boltzmann constant, T is solution temperature, η is fluid solution dynamic viscosity, ρ is fluid density, P_0 is atmospheric pressure, D is diffusion

coefficient of dissolved CO_2 molecules in the liquid and α is a numerical prefactor which is close to 0.7.

$$\Delta c = c_L - c_0$$

Here c_0 is equilibrium concentration of dissolved CO_2 molecules in the liquid medium corresponding to a pressure of CO_2 molecules in the vapor phase of 1 atm, and c_L is concentration of dissolved CO_2 molecules in the supersaturated liquid medium corresponding to a pressure of CO_2 molecules in 1.5 atm.

Supporting Information 20: Bubble CAs on the interfaces with different microstructures and chemical components.

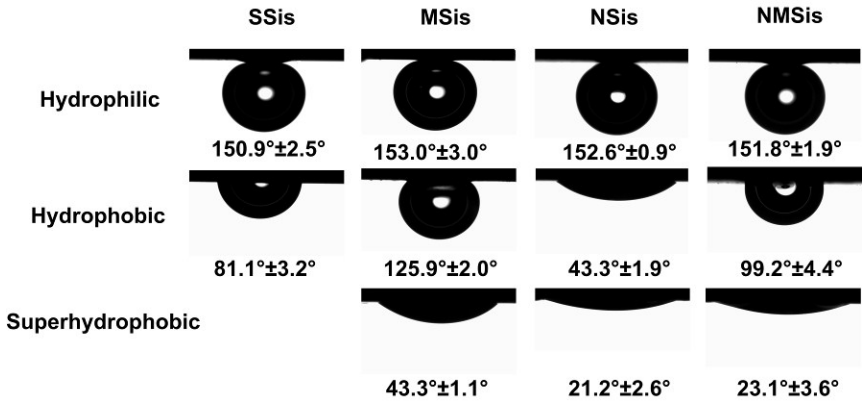

Fig. S19 Bubble CAs on the interfaces with different microstructures and chemical components.

Supporting Information 21: When the buoyancy of the gas bubble balances the wetting force, $\boldsymbol{F_w}=\boldsymbol{F_b}$,

$$6\gamma \sin^2\theta = \rho g R^2 (1+\cos\theta)^2 (2-\cos\theta)$$

$$6\gamma (1-\cos\theta) = \rho g R^2 (1+\cos\theta)(2-\cos\theta)$$

$$\because \cos\theta = \frac{1-\tan^2 \theta/2}{1+\tan^2 \theta/2}$$

$$\therefore R^2 = \frac{6\gamma}{\rho g}\frac{\tan^2 \theta/2\,(1+\tan^2 \theta/2)}{1+3\tan^2 \theta/2}$$

$$\therefore R^2 = \frac{6\gamma}{\rho g}\frac{\tan^2 \theta/2}{1+\dfrac{2}{1+\dfrac{1}{\tan^2 \theta/2}}}$$